

## Ultrafast dynamics of photoexcited coherent phonon in Bi<sub>2</sub>Te<sub>3</sub> thin films

Alexander Q. Wu and Xianfan Xu<sup>a)</sup>

School of Mechanical Engineering, Purdue University, West Lafayette, Indiana 47907, USA

Rama Venkatasubramanian

Center for Solid State Energetics, RTI International, Research Triangle Park, North Carolina 27709, USA

(Received 16 November 2007; accepted 6 December 2007; published online 3 January 2008)

Nonequilibrium  $A_{1g}$  longitudinal optical phonon with a frequency of 1.84 THz in bismuth telluride (Bi<sub>2</sub>Te<sub>3</sub>) is coherently excited by ultrafast pulses. Time-resolved reflectivity measurements show a distinct second harmonic vibration around 3.68 THz at room temperature caused by the nonlinearity of coherent phonon potentially related to the favorable crystal structure of Bi<sub>2</sub>Te<sub>3</sub>. The scattering rate between  $A_{1g}$  coherent phonon and room temperature incoherent phonon is derived from the pump-fluence-dependent scattering rate of  $A_{1g}$  coherent phonon. It is also observed that energy coupling from photoexcited carriers to lattice through coherent phonon vibration is more efficient and faster at higher pump fluence. © 2008 American Institute of Physics.

[DOI: 10.1063/1.2829604]

Dynamics of phonons and excited carriers are key parameters for the performance of technologically important devices. The excited carriers (electrons and holes), which are either pumped optically or electrically, will relax back to the ground states by scattering with phonons, boundaries, impurities, and so on. Time-resolved optical measurement is a unique way to study specific optical phonon mode as ultrafast pulses generate predominantly the  $A_{1g}$  coherent phonon vibration.<sup>1-3</sup> Compared with the Raman scattering technique, the time-resolved measurement offers real-time investigation of phonon dynamics with better signal-noise ratio and bandwidth resolution.<sup>4</sup> In this letter, we report the dynamics of  $A_{1g}$  optical phonon and photoexcited carriers in semiconductor Bi<sub>2</sub>Te<sub>3</sub>, which is an efficient thermoelectric material at room temperature,<sup>5</sup> by measuring the ultrafast time-resolved reflectivity.

A *p*-type single crystalline Bi<sub>2</sub>Te<sub>3</sub> film was grown by metal-organic chemical-vapor deposition on a GaAs (100) substrate.<sup>6</sup> The mobility  $\mu$  of the Bi<sub>2</sub>Te<sub>3</sub> film is 230 cm<sup>2</sup> V<sup>-1</sup> s<sup>-1</sup>. The film thickness is around 1.0  $\mu$ m, which is much thicker than the optical absorption depth ( $\sim$ 10 nm) at the 800 and 400 nm laser wavelengths employed in the experiments.<sup>7</sup> Time-resolved reflectivity measurements were performed at room temperature on the surface perpendicular to the trigonal axis by a standard collinear two-color pump-probe setup. The laser pulses were produced by a Spectra Physics regenerative amplifier system, which outputs 100 fs full width at half maximum pulses with energy up to 1 mJ/pulse at the center wavelength of 800 nm and a repetition rate of 1 kHz. The pump beam at a center wavelength of 400 nm was generated by a beta-BaB<sub>2</sub>O<sub>4</sub> (BBO) crystal. The residual 800 nm laser beam was blocked by a bandpass filter for wavelength of 400 $\pm$ 20 nm. The collinear 400 nm pump and 800 nm probe beams were normally focused on the sample surface by a 100 mm lens to diameters of 80 and 20  $\mu$ m, respectively. The reflected beam was collected by the focused lens and sent into a balanced detector with bandpass filters at 800 $\pm$ 20 nm wavelengths. An op-

tical chopper synchronized to the laser pulses was used to modulate the pump pulse, and the reflected beam signal was measured by a lock-in amplifier. The pump laser fluence was adjusted with a half wave plate and polarizer combination. The probe beam fluence was fixed at 0.02 mJ/cm<sup>2</sup>. A sum frequency generation crystal was used to measure the correlation of pump and probe beams.

Time-resolved measurement signals with several pump fluences are shown in Fig. 1. A damping oscillatory signal is superimposed onto a nonoscillatory signal. The oscillatory and nonoscillatory components can be separated by applying a digital low-pass filter on the experimental data. The Fourier transform in Fig. 1(b) shows the frequency of the oscillatory signals is centered at 1.84 THz, agreeing with the 1.88 THz frequency of  $A_{1g}$  longitudinal optical phonon measured by Raman scattering.<sup>8</sup> The oscillatory signal is attributed to the coherent phonon vibration generated by the pumping pulse through a process called displacive excitation of coherent phonon,<sup>3</sup> which is a limiting case of impulsive stimulated Raman scattering for opaque materials.<sup>9,10</sup> As the pump fluence is increased, the frequency of coherent phonon is slightly redshifted due to the softening effect caused by the photoexcited electrons.<sup>11,12</sup>

A unique observation in Fig. 1(b) is that a frequency around 3.68 THz appears as the pump fluence increased. We attribute this to the second harmonic vibration of  $A_{1g}$  coherent phonon. To the first order approximation, the reflectivity change due to the coherent phonon can be expressed as  $\Delta R/R = [(\partial\Delta R/R)/\partial Q]Q = [(\partial\Delta R/R)/\partial Q]AQ_0$ , where  $A$  is the amplitude of coherent phonon and  $Q_0$  is the normalized coordinate of coherent phonon modeled as a chirped damping harmonic oscillator,<sup>13,14</sup>

$$Q_0 = \exp(-\Gamma t) \cos[(\Omega + \beta t)t + \varphi], \quad (1)$$

where  $\Gamma$ ,  $\Omega$ ,  $\beta$ , and  $\varphi$  are scattering rate, angular frequency, chirping coefficient, and initial phase, respectively. As the coherent phonon amplitude is increased, the effect of higher order terms of coherent phonon coordinate on reflectivity becomes non-negligible. Considering the second order approximation, the reflectivity change is expressed as

<sup>a)</sup>Electronic mail: xxu@ecn.purdue.edu. Tel: 1-765-494-5639. FAX: 1-765-494-0539.

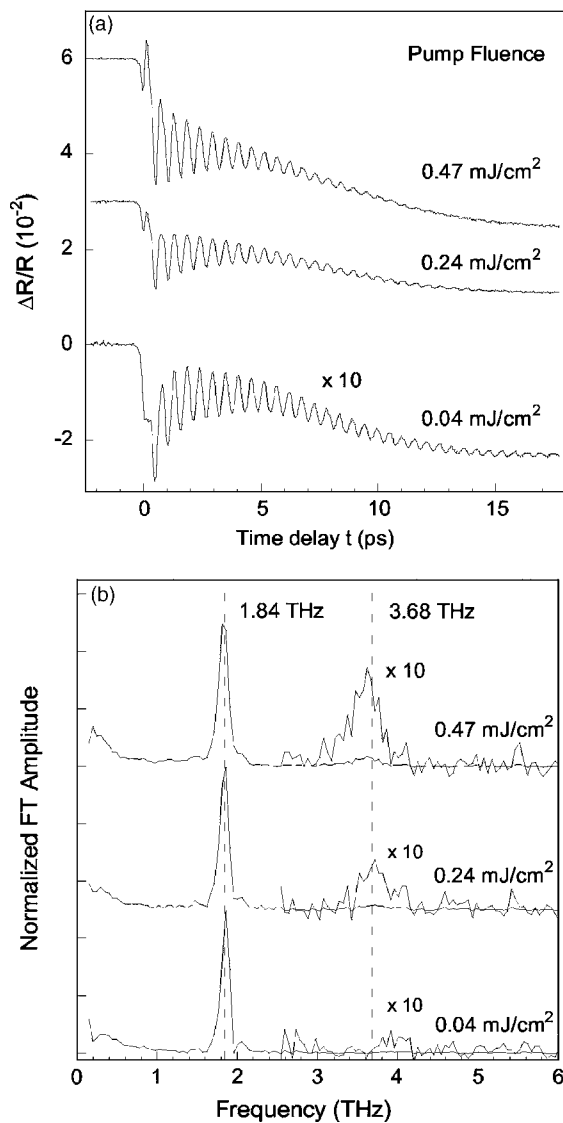


FIG. 1. (a) Time resolved reflectivity of  $\text{Bi}_2\text{Te}_3$  pumped by different laser fluences. The reflectivity measured with fluence of  $0.04 \text{ mJ/cm}^2$  is magnified ten times. (b) The corresponding frequency spectrum calculated by Fourier transforms, and the spectrum above  $2.5 \text{ THz}$  is magnified ten times for clarity. The curves are vertically translated and labeled with the pump fluence.

$$\frac{\Delta R}{R} = \frac{\partial \Delta R/R}{\partial Q} A Q_0 + \frac{1}{2} \frac{\partial^2 \Delta R/R}{\partial Q^2} A^2 Q_0^2. \quad (2)$$

The second order term  $Q_0^2$  generates an oscillation at second harmonic frequency  $2\Omega$  with a double scattering rate  $2\Gamma$ . Such a second harmonic (and higher harmonics) frequency was also observed in ultrafast measurements of Bismuth and  $\text{KTaO}_3$  at low temperature of  $10 \text{ K}$  and was attributed to either the Bose-Einstein condensation or the second order Raman scattering.<sup>14–16</sup> Noticeably, in our experiments, the second harmonic vibration of coherent phonon was observed at room temperature rather than at low temperature. It is possible that this second harmonic generation at room temperature is due to the crystal structure  $\text{Bi}_2\text{Te}_3$  along the  $c$  axis with the periodic van der Waal bonds, which is more efficient for coherent phonon generation.

The signal of coherent phonon is obtained by subtracting the nonoscillatory component from the reflectivity change and is shown in Fig. 2. Then, the coherent phonon signal is modeled as

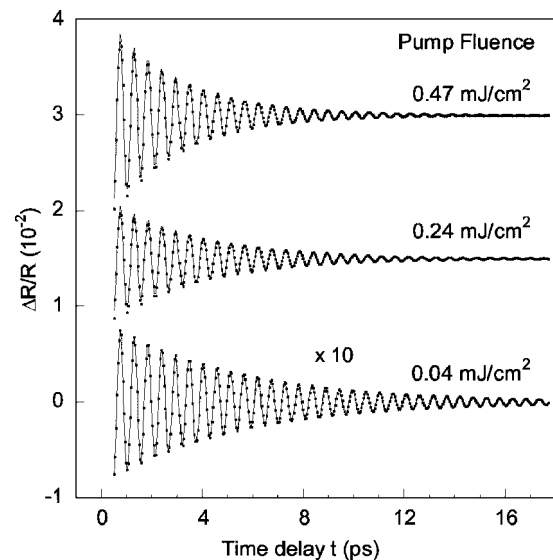


FIG. 2. Oscillatory signal of coherent phonon after  $0.5 \text{ ps}$  delay. The dots are experimental data and the lines are fitted curves.

$$\frac{\Delta R}{R} = A_1 Q_0 + A_2 Q_0^2, \quad (3)$$

where  $A_1$  and  $A_2$  are reflectivity change induced by the primary and second harmonic coherent phonons, respectively. In order to reduce the distortion effect resulting from the digital low-pass filter, we only consider the data fitting after  $0.5 \text{ ps}$  delay. The scattering rate  $\Gamma$  is essentially the inverse of the coherent phonon dephasing time, which is about a few picoseconds, as shown in Fig. 2. The pump fluence dependence of fitted amplitudes and scattering rates are shown in Fig. 3. Below  $0.32 \text{ mJ/cm}^2$ , both amplitude and scattering rate of the primary coherent phonon are linear with the pump fluence.

The linear dependence of scattering rate on pump fluence can be explained by the linear increase of photoexcited carriers. The incident laser pulse initially generates photoexcited carriers,<sup>17</sup> which then redistribute energy through coherent phonon generation, electron-phonon coupling, carrier diffusion, and electron-hole recombination. The pumping laser of  $3.1 \text{ eV}$  does not resonantly excite the carriers in  $\text{Bi}_2\text{Te}_3$  with an indirect band gap of  $0.15 \text{ eV}$ ,<sup>18</sup> therefore the excess kinetic energy of the excited carriers (hot carriers) after interband transition will rapidly release energy by emitting incoherent phonons through electron-phonon coupling. Both the increases of photoexcited carriers and emitted incoherent phonons are linearly dependent on the pump fluence, resulting in a linearly increased scattering rate of coherent phonon shown in Fig. 3(b). By extrapolating the pump fluence dependent scattering rate to zero pump fluence, we obtain a scattering rate of  $0.18 \text{ THz}$ , which is the scattering rate caused by the background incoherent phonons at room temperature.

The nonoscillatory signal is due to the photoexcited carriers and lattice heating.<sup>13</sup> At weak pump fluence in Fig. 1, there is an appreciable initial decrease of the (nonoscillatory) signal caused by photon excitation of hot carriers, followed by the signal recovery after  $0.5 \text{ ps}$  with a signal recovery time (or decay time) around  $0.6 \text{ ps}$ . Both thermalization of hot carriers through electron-phonon coupling and carrier diffusion can contribute to the decay process. The ambipolar

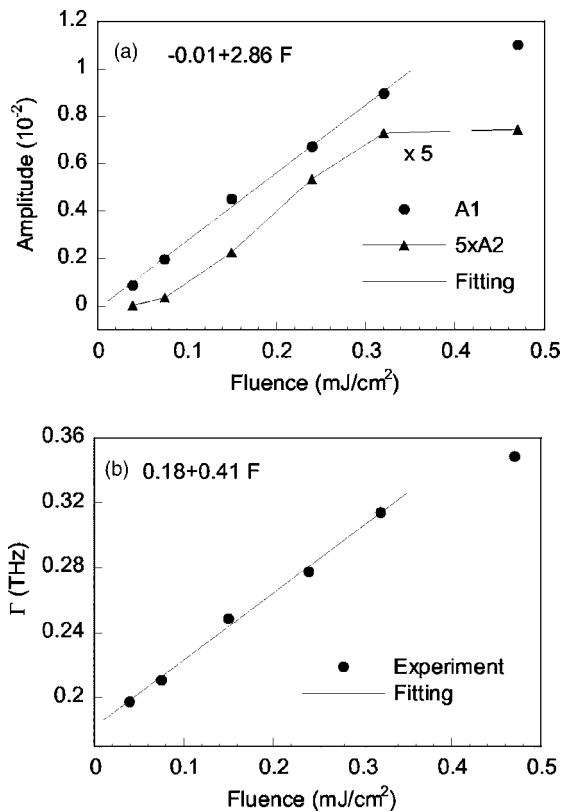


FIG. 3. Pump fluence dependence of (a) reflectivity amplitudes induced by the primary and second harmonic coherent phonons, and (b)  $A_{1g}$  scattering rate  $\Gamma$ . Note: the fitting without considering the second harmonic vibration shows similar results.

diffusion of photoexcited carrier density  $\rho$  can be modeled using the diffusion equation

$$\frac{\partial \rho}{\partial t} = D \frac{\partial^2 \rho}{\partial z^2} + \frac{(1-R)F}{\xi \tau q} e^{-(t/\tau)^2} e^{-z/\xi}, \quad (4)$$

where  $R$ ,  $F$ ,  $\xi$ ,  $\tau$ , and  $q$  are reflectivity, laser fluence, optical absorption depth, pulsewidth, and photon energy of pump beam, respectively.  $D$  is the ambipolar diffusion coefficient, which can be derived from the mobility value  $\mu$  by the Einstein relation  $D = (kT/e)\mu$ ,<sup>19</sup> where  $k$ ,  $T$ , and  $e$  are the Boltzmann constant, temperature, and electron charge, respectively. The solution of Eq. (4), the normalized time-dependent carrier density at  $z=0$ , 4.9, and 9.8 nm is shown in Fig. 4. It is seen that the carrier density decay caused by diffusion occurs at a time scale of about 1 ps, while the measured carrier decay time is 0.6 ps. This shows both carrier diffusion and thermalization of hot carriers contribute to the rapid carrier decay. As the pump fluence increased, the signal due to the photoexcited carriers is buried in the signals of coherent phonon vibration because of the increased coherent phonon vibration. The amplitude of coherent phonon vibration is almost linear with pump fluence, as shown in Fig. 3(a); therefore the corresponding coherent phonon energy is proportional to the square of pump fluence. The scattering rate of coherent phonon also varies linearly with pump fluence, as shown in Fig. 3(b). As such, the energy coupling from photoexcited carriers to the lattice through coherent phonon vibration is more efficient and much faster (i.e., a larger scattering rate), covering the decay signal of the photoexcited carriers at high pump fluence.

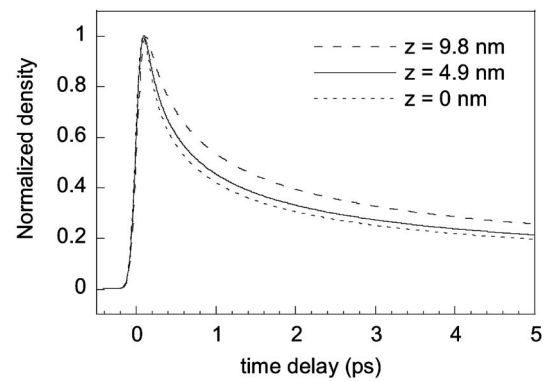


FIG. 4. Time dependence of normalized density at different  $z$  positions due to ambipolar diffusion based on Eq. (4) with  $D=6$  cm<sup>2</sup>/s,  $R=0.74$ ,  $F=0.04$  mJ/cm<sup>2</sup>,  $\xi=9.1$  nm,  $\tau=0.084$  ps, and  $q=3.1$  eV. The optical absorption depth of 800 nm probe beam is 9.8 nm.

In summary, we reported time-resolved reflectivity of semiconductor Bi<sub>2</sub>Te<sub>3</sub>. A second harmonic frequency around 3.68 THz was observed and attributed to the nonlinearity of coherent phonon vibration excited in the film. The scattering rate of coherent phonon was found to linearly increase with the pump fluence, and a 0.18 THz scattering rate of incoherent phonons was derived from pump fluence dependent experiments. It is also found that the energy coupling from photoexcited electrons to lattice through coherent phonon vibration is more efficient and faster at high pump fluence.

Support to this work by the National Science Foundation and Sandia National Laboratory is acknowledged. The Bi<sub>2</sub>Te<sub>3</sub> thin-film materials were produced at RTI International under a DARPA/DSO funded effort; this ONR Navy under Contract No. N00014-04-C-0042 is gratefully acknowledged.

- <sup>1</sup>T. K. Cheng, S. D. Brorson, A. S. Kazeroonian, J. S. Moodera, G. Dresselhaus, M. S. Dresselhaus, and E. P. Ippen, *Appl. Phys. Lett.* **57**, 1004 (1990).
- <sup>2</sup>T. K. Cheng, J. Vidal, H. J. Zeiger, G. Dresselhaus, M. S. Dresselhaus, and E. P. Ippen, *Appl. Phys. Lett.* **59**, 1923 (1991).
- <sup>3</sup>H. J. Zeiger, J. Vidal, T. K. Cheng, E. P. Ippen, G. Dresselhaus, and M. S. Dresselhaus, *Phys. Rev. B* **45**, 768 (1992).
- <sup>4</sup>Y. X. Yan and K. A. Nelson, *J. Chem. Phys.* **83**, 5391 (1986).
- <sup>5</sup>F. J. DiSalvo, *Science* **285**, 703 (1999).
- <sup>6</sup>R. Venkatasubramanian, T. Colpitts, E. Watko, M. Lamvik, and N. ElMasry, *J. Cryst. Growth* **170**, 817 (1997).
- <sup>7</sup>D. L. Greenaway and G. Harbeke, *J. Phys. Chem. Solids* **26**, 1585 (1965).
- <sup>8</sup>W. Richter, H. Köhler, and C. R. Becker, *Phys. Status Solidi B* **84**, 619 (1977).
- <sup>9</sup>G. A. Garrett, T. F. Albrecht, J. F. Whitaker, and R. Merlin, *Phys. Rev. Lett.* **77**, 3661 (1996).
- <sup>10</sup>T. E. Stevens, J. Kuhl, and R. Merlin, *Phys. Rev. B* **65**, 144304 (2002).
- <sup>11</sup>A. Q. Wu and X. Xu, *Appl. Surf. Sci.* **253**, 6301 (2007).
- <sup>12</sup>S. Hunsche, K. Wienecke, T. Dekorsy, and H. Kurz, *Phys. Rev. Lett.* **75**, 1815 (1995).
- <sup>13</sup>A. Q. Wu and X. Xu, *Appl. Phys. Lett.* **90**, 251111 (2007).
- <sup>14</sup>O. V. Misocho, M. Hase, K. Ishioka, and M. Kitajima, *Phys. Rev. Lett.* **92**, 197401 (2004).
- <sup>15</sup>G. A. Garrett, A. G. Rojo, A. K. Sood, J. F. Whitaker, and R. Merlin, *Science* **275**, 1638 (1997).
- <sup>16</sup>A. Bartels, T. Dekorsy, and H. Kurz, *Phys. Rev. Lett.* **84**, 2981 (2000).
- <sup>17</sup>A. Q. Wu, I. H. Chowdhury, and X. Xu, *Phys. Rev. B* **72**, 085128 (2005).
- <sup>18</sup>R. Clasen, P. Grosse, A. Krost, and F. Levy, *Non-Tetrahedrally Bonded Elements and Binary Compounds I*, Landolt-Bornstein, New Series, Group III, Vol. 17, Pt. B, 1st ed. (Springer, New York, 1998).
- <sup>19</sup>O. B. Wright, B. Perrin, O. Matsuda, and V. E. Gusev, *Phys. Rev. B* **64**, 081202 (2001).